JBMR Plus, 2025, **9**, ziae179
https://doi.org/10.1093/jbmrpl/ziae179
Advance access publication: January 8, 2025
Case Report

Paradoxical combination of osteosclerosis and osteopenia in an adult woman with biallelic *TNFRSF11A* loss-of-function variants escaping nonsense-mediated decay

Dario Gajewski[1], Anna Floriane Hennig[1], Regina Grün[1], Heide Siggelkow[2,3], Svenja Vishnolia[1], Leonard Bastian[4], Hanna Taipaleenmäki[5,6], Ansgar Schulz[7], Uwe Kornak[1,2], Eric Hesse[5,6,*]

[1]Institute of Human Genetics, University Medical Center Göttingen, 37073 Göttingen, Germany
[2]MVZ Endokrinologikum Göttingen, 37075 Göttingen, Germany
[3]Department of Trauma, Orthopedics and Reconstructive Surgery, University Medical Center Göttingen, 37075 Göttingen, Germany
[4]Department of Orthopedics and Trauma Surgery, Hospital Leverkusen, 51375 Leverkusen, Germany
[5]Institute of Musculoskeletal Medicine, LMU University Hospital, LMU Munich, 82152 Planegg-Martinsried, Germany
[6]Musculoskeletal University Center Munich, LMU University Hospital, LMU Munich, 82152 Planegg-Martinsried, Germany
[7]Department of Pediatrics, University Medical Center Ulm, 89075 Ulm, Germany

*Corresponding author: Eric Hesse, Institute of Musculoskeletal Medicine, LMU University Hospital, LMU Munich, Fraunhoferstr. 20, 82152 Planegg-Martinsried, Germany (Eric.Hesse@med.uni-muenchen.de).

Abstract

Osteoclasts are essential for bone resorption, playing a crucial role in skeletal development, homeostasis, and remodeling. Their differentiation depends on the RANK receptor encoded by the *TNFRSF11A* gene, with defects in this gene linked to osteoclast-poor sclerosing skeletal dysplasias. This report presents a 37-yr-old woman with normal height, valgus deformities that were treated surgically, frequent fractures, scoliosis, mildly elevated BMD, sclerotic diaphyseal bone, and metaphyseal widening. Initially suspected of having dysosteosclerosis, her diagnosis shifted toward Pyle disease due to the valgus deformity and prominent metaphyseal widening and translucency. Genetic analysis identified 2 pathogenic *TNFRSF11A* variants: a nonsense mutation c.1093G>T, p.(Glu365*) and a frameshift mutation c.1266_1268delinsCC, p.(Leu422Phefs*104). Thus, genetic and clinical assessment converged on the diagnosis of a mild form of dysosteosclerosis. Both mutations introduced premature stop codons but escaped complete nonsense-mediated decay, potentially permitting residual protein function. Analysis of patient-derived osteoclasts cultured on glass surfaces showed partial differentiation. However, in vitro resorptive function was strongly impaired, which was clinically reflected by reduced serum concentration of the bone resorption marker CTx. Despite this impairment, the retained residual resorptive function likely explains the patient's relatively mild clinical presentation. These findings underscore the complex genetic interactions that affect osteoclast function, leading to a spectrum of phenotypes in osteoclast-related bone disorders.

Keywords: dysosteosclerosis, Pyle disease, RANK mutation, osteoclast, cortical bone, fracture, nonsense-mediated decay

Lay Summary

Osteoclasts are vital for maintaining bone health by breaking down bone tissue. This report describes a 37-yr-old woman diagnosed with dysosteosclerosis; a condition caused by mutations in the *TNFRSF11A* gene that impair bone resorption. She experienced scoliosis and frequent fractures from minor injuries. Initially suspected of having Pyle disease due to specific bone defects, genetic testing confirmed dysosteosclerosis with 2 mutations identified. Despite her milder symptoms, she faced numerous fractures. This case provides insights into the link between genetic mutations and bone disorders, highlighting the complexity of bone remodeling mechanisms.

Received: October 31, 2024. **Revised:** November 29, 2024. **Accepted:** January 7, 2025

Graphical Abstract

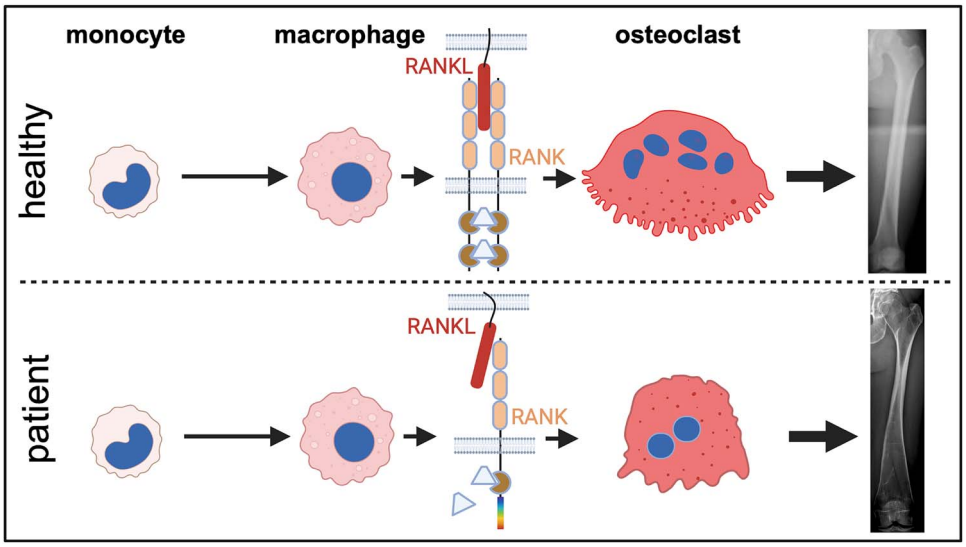

Introduction

Osteoclasts are the only cells capable of resorbing mineralized cartilage and bone tissue. During skeletal development, osteoclasts resorb large amounts of mineralized tissue to facilitate bone growth, modeling, and remodeling. After growth stops, bone turnover decreases, and osteoclasts primarily function in remodeling, repairing local damage, and regulating calcium during skeletal homeostasis.[1]

Osteoclast differentiation depends on the interaction between the RANK receptor on hematopoietic osteoclast precursors and RANKL, which is produced by immune cells, osteoblasts, and osteocytes. RANKL can exist on cell surfaces or in a soluble form following proteolytic shedding.[1]

Osteopetrosis is a group of skeletal dysplasias characterized by impaired bone resorption.[2,3] It is classified into 2 major subtypes: osteoclast-rich and osteoclast-poor. Dysosteosclerosis (OMIM #224300) is mainly categorized under osteoclast-poor osteopetrosis and is associated with mutations in genes such as *CSFR1*, *TNFRSF11A*, and *SLC29A3*.[4] This rare disorder can present with reduced long bone growth, metaphyseal sclerosis, metaphyseal widening (resulting in the characteristic Erlenmeyer-shaped femora), small diaphyses with irregular cortices, and flattened vertebrae with sclerotic endplates. Patients are prone to fractures, and early visual impairment due to optic nerve damage.[5] Later stages show metaphyseal translucency and cortical thinning, resembling Pyle disease (OMIM #265900), a feature absent in other osteopetrosis forms.[6] Unlike severe autosomal recessive osteopetrosis (ARO), dysosteosclerosis does not impair bone marrow (BM) function.

Multiple biallelic nonsense, frameshift, and missense mutations in *TNFRSF11A* have been linked to severe ARO with B-cell impairment.[7,8] Similar mutations have been found in individuals with dysosteosclerosis,[9–11] with milder phenotypes likely due to residual *TNFRSF11A* function, as some transcripts escape nonsense-mediated decay (NMD).

In this report, we present an adult female patient with osteopenia and distinct metaphyseal widening presumably due to remodeling defects, with Pyle disease and dysosteosclerosis considered as potential diagnoses. The patient was found to be compound heterozygous for *TNFRSF11A* mutations. Functional analysis of these variants, compared to ARO caused by a homozygous *TNFRSF11A* frameshift mutation, provides new insights into the pathogenesis of dysosteosclerosis.

Patient case

A 37-yr-old woman presented with a history of bone deformities, scoliosis, and fractures, primarily from low- or no-energy trauma, which became more frequent with age. In childhood, she developed bilateral valgus deformities (Figure 1A), which were corrected through multiple osteotomies and epiphysiodesis, resulting in straight leg axes (Figure 1B and C). She exhibited scoliosis (Figure 1C and D), with several deformed thoracic and lumbar vertebrae, though without classic platyspondyly. Radiographs showed increased radiodensity in the vertebral endplates without the typical sandwich conformation (Figure 1D). Persistent metaphyseal widening with thin cortices was observed at the distal radius (Figure 1E), proximal humerus (Figure 1F), and proximal femora (Figure 1G). Additionally, the femora exhibited diaphyseal cortical thickening and sclerosis, with an Erlenmeyer shape (Figure 1H). There was also metaphyseal widening with thin cortices and diffuse sclerotic zones in the trabecular compartment (Figure 1I).

Throughout adolescence and adulthood, she suffered multiple fractures, including those in the distal radius, pelvic ring, metatarsals, ribs, fingers, toes, navicular bone, skull, scapula, olecranon, and tibiae. The tibiae also showed diaphyseal sclerosis with metaphyseal widening and thin cortices (Figure 1J). Recently, she underwent plate osteosynthesis for a peri-implant fracture of the left tibia, which had not fully healed by her presentation (Figure 1K).

She experienced post-surgical left big toe dorsiflexion paresis, bilateral hallux valgus, autoimmune thyroiditis, and is HLA-B27-positive. At presentation, her symptoms included back pain due to thoracolumbar scoliosis, chronic musculoskeletal pain, and impaired mobility. She is currently taking vitamin D3 (20 000 IU/wk) and levothyroxine (125 μg/d).

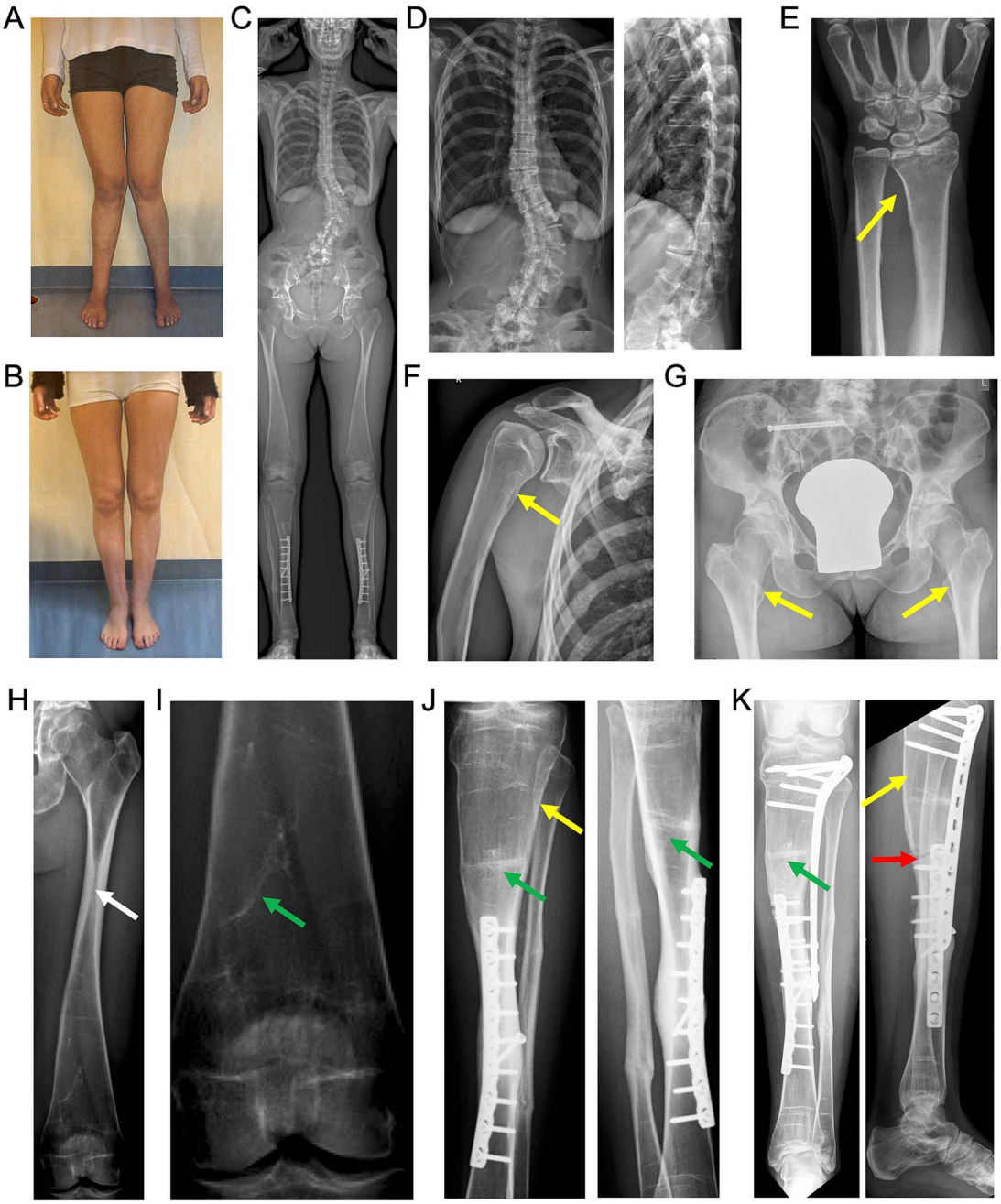

Figure 1. Clinical and radiographic presentation of skeletal abnormalities. (A) Photograph showing valgus deformity in childhood. (B) Photograph of the legs after orthopedic correction of the valgus deformities. (C) Whole-body X-ray demonstrating straight leg axes following tibial osteotomies and scoliosis. (D) X-ray of the thoracic and LS, with anterior-posterior (left) and lateral (right) views showing scoliosis with opaque endplates but no platyspondyly. Metaphyseal widening (yellow arrow) is evident in X-rays of (E) the left lower arm postfracture, (F) the right proximal humerus, and (G) the proximal femora and pelvis, where screw osteosynthesis was applied after a pelvic ring fracture. (H) Magnified view of the left femur from panel (C) showing diaphyseal sclerosis due to thick cortical bone (white arrow), along with thinning and widening of the metaphyses, resulting in an Erlenmeyer shape. (I) Magnified view of the left distal femur from (H) displaying diffuse sclerosing trabecular patterns (green arrow). X-rays of the left tibia, with anterior-posterior (left) and lateral (right) views (J) show the previous plate osteosynthesis and (K) recent osteosynthesis after a peri-implant fracture. The fracture was not yet healed by the time of examination, with a visible gap (red arrow). Structural alterations such as diaphyseal cortical thickening, metaphyseal widening with thin cortices, and diffuse medullary sclerosis (green arrows) are also observed in the tibiae (J, K).

In childhood, there was uncertainty between a diagnosis of dysosteosclerosis and Pyle disease, with the latter initially favored. Her mother and grandmother have scoliosis but are otherwise healthy, as is her father. Her 2-yr-old son shows no clinical symptoms and is highly unlikely to be affected by the disease.

On examination, she measured 172.5 cm in height (75. percentile), weighed 66 kg, and had a BMI of 22.05 kg/m^2. She had no cranial nerve palsies, optic nerve damage, or cognitive deficits. Scoliosis with resulting stiffness of the back muscles and a pelvic tilt were noted. Her fingertip-to-floor distance was 20 cm. Hand grip strength, tandem stand, and the timed-up-and-go test showed no muscle weakness. DXA revealed the following BMD results: For the left proximal femur, a BMD *T*-score of 0.0 (1.005 g/cm^2) and a Z-score of 0.1 were observed. The right proximal femur showed a

Table 1. Overview of selected serum parameters.

Parameter	Value	Unit	Reference range	Change
PTH	3.39	pmol/L	1.83-7.85	-
25-OH vitamin D3	99	nmol/L	75-100	-
γ-GT	11.1	U/L	<40	-
Alkaline phosphatase	58	U/L	35-104	-
Bone-specific alkaline phosphatase	9.0	μg/L	<27.1	-
Glomerular filtration rate	20.4	ml/min/1.73 m^2	>60	-
Sodium	16.5	mmol/L	136-145	-
Calcium	2.3	mmol/L	2.15-2.50	-
Phosphate	1.29	mmol/L	0.81-1.45	-
Osteocalcin	18.3	μg/L	6.5-42.3	-
Undercarboxylated osteoclacin	4.7	ng/mL	0.6–3.3	↑
P1NP	26.2	ng/mL	27.7-127.6	↓
CTx	0.06	μg/L	0.15-0.64	↓
CRP	<1.0	mg/L	<5.0	-
Basal TSH	4.16	mIU/L	0.4-4.0	↑
Thyroid peroxidase antibodies	1349	U/mL	<60	↑

Abbreviation: CRP, C-reactive protein.

BMD *T*-score of 1.2 (1.146 g/cm^2) and a Z-score of 1.4. The DXA scan's limitations include irregular proximal femur morphology that could have influenced the measurement. Due to scoliosis and opaque endplates, BMD could not be determined at the LS.

Laboratory tests revealed normal serum concentrations of PTH, 25-OH vitamin D3, γ-GT, alkaline phosphatase, bone-specific alkaline phosphatase, glomerular filtration rate, sodium, calcium, phosphate, and C-reactive protein (Table 1). Basal Thyroid stimulating hormone (TSH) was elevated, along with thyroid peroxidase antibodies, likely due to the patient's known thyroid disease. While the bone formation marker osteocalcin was within normal range, undercarboxylated osteocalcin was elevated, suggesting a functional vitamin K deficiency. P1NP, another bone formation marker, was slightly reduced. Notably, the bone resorption marker CTx was markedly reduced, indicating severely impaired bone resorption (Table 1). No abnormalities were found in the full blood count, serum protein electrophoresis, immunofixation, iron metabolism, liver and lipid metabolism, vitamins (including B12, K1, and K2), or hormones, including sex hormones (data not shown).

Materials and methods

Genetic analysis

A blood sample was collected in EDTA for DNA isolation. Following library preparation, we used the custom-designed SureSelect XT skeletal disease-associated genome gene panel (Agilent) to isolate coding exons of genes linked to skeletal dysplasias, dysostoses, and connective tissue disorders.[12] Sequencing was performed on a NextSeq platform (Illumina) and analyzed through standard bioinformatics pipelines. Variants were filtered by frequency and pathogenicity and prioritized based on phenotype relevance using MutationDistiller[13] and MutationTaster.[14] Genetic variants were classified following the American College of Medical Genetics and Genomics (ACMG) guidelines.[15] Variants were segregated by standard Sanger sequencing using primers described in Table S1.

Osteoclast culture and analysis

Mononucleated cells were isolated from heparinized blood samples of patients and controls by density gradient centrifugation using Histopaque 1077 (Sigma Aldrich). $CD14^+$ monocytes were then separated using the PAN monocyte isolation kit and LS columns (Miltenyi Biotec). Cells were cultured in osteoclast medium, composed of MEM Alpha Eagle modification (PAN Biotech), supplemented with 10% FBS Superior (Sigma Aldrich), 1% GlutaMax and 1% penicillin/streptomycin (both Gibco) and 30 ng/mL M-CSF (Bio-Techne). For staining, cells were plated on tissue-culture-treated (TC) plastic 12-well plates (Corning Life Sciences) or 8-well glass chamber slides (ibidi). For RNA and protein isolation, cells were seeded in tissue culture plastic 12- or 6-well plates. To assess bone resorption, cells were seeded in a density of 6×10^4 cells/well in 96-well plates on bovine cortical bone slices (boneslices.com). After 3 d, half of the medium was replaced with osteoclast medium containing 60 ng/mL M-CSF and 100 ng/mL RANKL (PeproTech), with medium changes every 2-3 d. Cells were cultured at 37°C and 5% CO_2 in a humidified incubator.

Qunatitative RT-PCR

RNA was isolated using the AllPrep Mini Kit (Qiagen). For cDNA synthesis, 1 μg RNA was reverse transcribed with the First Strand cDNA Synthesis Kit (Thermo Fisher Scientific). The resulting cDNA was diluted 1:50 for quantitative PCR (qPCR). qPCR was conducted in 384-well plates using the QuantiNova SYBR Green PCR Kit (Qiagen) on a QuantStudio5 system (Applied Biosystems). Data analysis followed the $\Delta\Delta C_T$ method. First, *POLR2G* expression, encoding the RBP7 subunit of RNA polymerase II, was used for normalization. The average ΔC_T of control samples was then subtracted from that of the test samples. Fold change was calculated using the $2^{-\Delta\Delta CT}$ formula. Primers are listed in Table S1.

CTx-I ELISA

The concentration of CTx-I in cell culture supernatants was measured using the CrossLaps for Culture CTx-I ELISA (Immunodiagnostic Systems). Supernatants were collected 10 d after osteoclast formation from bone resorption experiments, with medium from eight bone chips pooled for analysis. Culture medium alone was used as a blank and its values were subtracted from all samples.

Tartrate-resistant acid phosphatase assay

The concentration of tartrate-resistant acid phosphatase (TRAP) in cell culture supernatants was measured using a

Table 2. Comparison of clinical features with *TNFRSF11A*-associated dysosteosclerosis and Pyle disease.

Clinical manifestations (HPO terms)	Patient	TNFRSF11A- DOS[a] (no. of cases with feature/all cases)	Pyle disease
Sclerotic vertebral endplates (HP:000457)	Mild	4/4	0
Flattened vertebrae (HP:0000926)	Scoliosis	4/4	0
Metaphyseal under-modelling (HP:6001098)	1	4/4	1
Osteosclerosis of the calvaria and base of the skull (HP:0005746)	nd	4/4	0
Thickened ribs (HP:0000900)	1	4/4	1
Thinning of metaphyseal cortical bone after childhood	1	2/2	1
Pathologic fractures (HP:0002756)	1	3/4	1
Abnormality of the teeth (HP:0000164)	0	3/4	1
Short stature (HP:0004322)	0	3/4	0
Optic nerve compression (HP:0007807)	0	3/4	0
Mild global developmental delay (HP:0011342)	0	2/3	0
Recurrent infections (HP:0002719)	0	2/3	0
Anemia (HP:0001903)	0	1/3	0
Hepatosplenomegaly (HP:0001433)	0	1/4	0

0 = absent, 1 = present, nd = not determined. [a] Turan S., Bone, 2023 Feb 1;167.

colorimetric assay. Supernatants were collected 10 d after osteoclast formation in bone resorption experiments. In a 96-well plate, 50 μL each supernatant was combined with 150 μL TRAP buffer (7.6 mM *para*-Nitrophenylphosphat, 100 mM sodium acetate buffer pH 5.5, and 50 mM sodium tartrate) and incubated for 1 h at 37°C. The reaction was stopped by adding 50 μL of 3 M NaOH. Control samples were prepared by mixing supernatant with TRAP buffer and NaOH without incubation. All reactions were performed in triplicate. Absorbance was measured at 450 nm using an EPOCH2 microplate spectrophotometer (BioTek).

Osteoclast staining

Osteoclast cultures were fixed with 4% formaldehyde, followed by TRAP staining. Cells were incubated with 10 mg/mL Naphtol-AS-MX-phosphate in NN-dimethyl formamide diluted 1:1000 in TRAP buffer (40 mM sodium acetate, 10 mM sodium tartrate, pH 5.0), and supplemented with 0.42 mg/mL FastRed Violet LB salt (all chemicals from Sigma Aldrich) for 45 min at 37°C. After TRAP staining, cells were washed and permeabilized with 0.1% saponin in 3% BSA/PBS for 20 min. Cells were stained overnight with phalloidin Alexa Fluor 488 (1:400, Thermo Fisher Scientific), washed, and counterstained with 4',6-diamidino-2-phenylindolone (DAPI) for 10 min. in 3% BSA/PBS. After a final wash, cells were mounted using Fluoromount-G (SouthernBiotech), and images were captured with a Revolve microscope (Echo).

Statistical analysis

Data were analyzed using Graph Pad Prism 10. Mann–Whitney test was performed to determine statistical significance.

Results

Genetic analysis reveals compound heterozygous mutations in TNFRSF11A

Dysosteosclerosis was initially suspected, but Pyle disease was later favored due to the patient presenting clinical features partially consistent with both conditions, making the diagnosis unclear (Table 2). By gene panel sequencing the heterozygous variants c.1093G>T p.(Glu365*) and c.1266_1268delinsCC p.(Leu422Phefs*104) were identified in exon 9 of the gene *TNFRSF11A* (Figure 2A). Both variants were classified as pathogenic based on the ACMG criteria PVS1, PM2, and PP4.

Segregation analysis proved compound heterozygosity as the nonsense variant c.1093G>T was inherited paternally and the frameshift variant c.1266_1268delinsCC was inherited maternally (Figure 2B). Neither variant was present in control population databases, though the frameshift variant is listed in the ClinVar database (Accession: VCV000817702.2). Both variants are predicted to truncate the intracellular part of the RANK receptor (Figure 2C). The variant p.(Glu365*) likely eliminates both TRAF6 binding domains, while p.(Leu422Phefs*104) preserves one TRAF6 binding domain but introduces 104 additional random amino acids at the C-terminus. Since biallelic variants in *TNFRSF11A* leading to a frameshift or a PTC had previously been described to cause autosomal recessive dysosteosclerosis, the clinical diagnosis suspected initially was confirmed.

Impaired osteoclast differentiation and function

$CD14^+$ monocytes were isolated from PBMCs and differentiated into osteoclasts in vitro, with patient-derived cells compared to healthy controls. After 12-14 d of differentiation, patient-derived monocytes formed only a few multinucleated, osteoclast-like cells when cultured on tissue culture plastic (Figure 3A). However, when cultured on glass coverslips, the morphological differences were less pronounced, with multinucleated, TRAP-positive and phalloidin-positive actin rings observed, similar to control osteoclasts (Figure 3A). TRAP activity in the culture supernatant was comparable to controls (Figure 3B). Resorption pit analysis revealed minimal resorptive function (Figure 3C).

Correspondingly, concentrations of the bone resorption marker CTx were significantly reduced after culture on bovine bone slices (Figure 3D). This impaired osteoclast function aligns with findings from a previously reported case of *TNFRSF11A*-associated ARO due to the frameshift mutation c.328dupC in exon 4 (Figure S1A).[7] Also in this case, PBMCs formed a few osteoclast-like cells when differentiated on glass surfaces (Figure S1B). Overall, these results confirm that osteoclast function is severely compromised, even though some osteoclast formation remains intact.

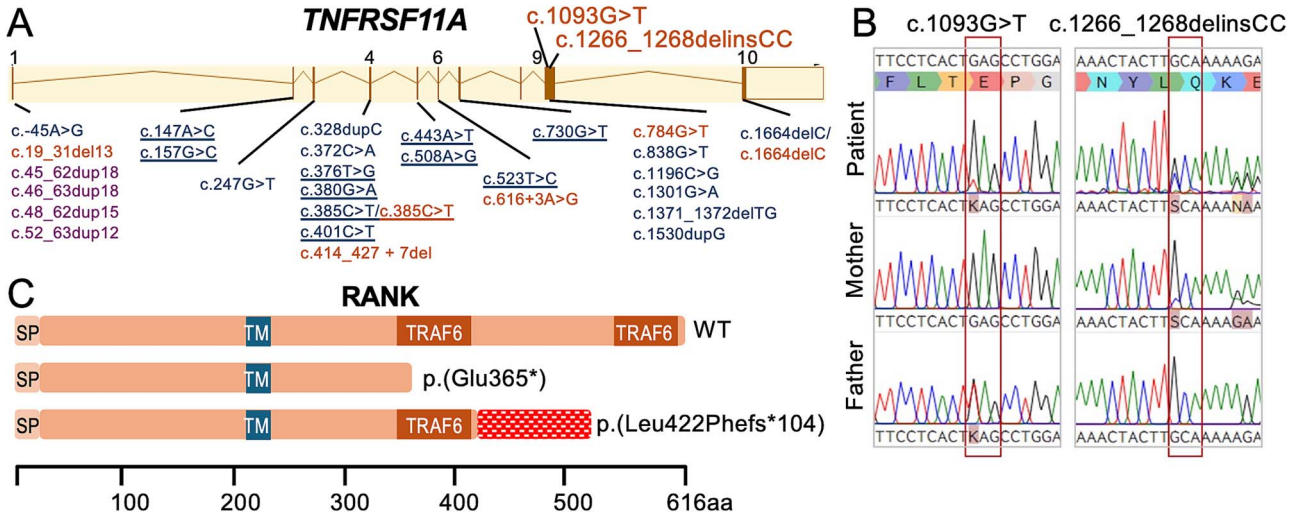

Figure 2. Variants in *TNFRSF11A* and their impact on the RANK protein. (A) Overview of disease-causing variants in *TNFRSF11A*. The upper section illustrates the gene structure, highlighting the 2 newly identified variants in exon 9. The lower section displays known pathogenic *TNFRSF11A* variants, including missense variants (underlined) and loss-of-function (LOF) variants. These variants result in diverse clinical phenotypes, including autosomal recessive osteopetrosis (blue), dysosteosclerosis (orange), and familial expansile osteolysis along with related disorders (purple). The variant list was obtained from the human gene mutation database (HGMD professional 2024.3) as of October 2024, supplemented by literature research. (B) Segregation analysis of the 2 variants in exon 9 of *TNFRSF11A*. The nonsense variant c.1093G>T (p.Glu365*) was inherited from the father, while the frameshift variant c.1266_1268delinsCC (p.Leu422Phefs*104) was inherited from the mother, confirming compound heterozygosity in the patient. (C) Predicted effects of the identified *TNFRSF11A* variants on the RANK protein. The nonsense variant p.(Glu365*) is expected to truncate the intracellular portion of the receptor, potentially eliminating both TRAF6 binding domains. In contrast, the frameshift variant p.(Leu422Phefs*104) retains one TRAF6 binding domain but introduces 104 random amino acids at the C-terminus.

Mildly reduced TNFRSF11A mRNA abundance and absence of alternative splice products

Both pathogenic variants are located in exon 9 of the *TNFRSF11A* gene, the second-to-last exon. Typically, variants introducing premature stop codons trigger NMD. However, quantitative RT-PCR from patient-derived osteoclast mRNA showed only a ~25% reduction in *TNFRSF11A* expression (Figure 4A). Additionally, expression of osteoclast differentiation markers *CTSK*, *MMP9*, and *NFATC1* was strongly reduced, confirming a differentiation defect (Figure 4B).

Inefficient NMD for *TNFRSF11A* premature stop codons has been explained by alternative transcripts unaffected by the mutations.[8] To investigate this, we amplified *TNFRSF11A* cDNA by RT-PCR using 2 different primer sets. Both yielded a single major product with no significant alternative transcripts (Figure 4C). Sequencing confirmed both mutations, each present at roughly 50% peak height, suggesting limited NMD activity. Furthermore, exon-exon junctions between exons 9, 8, and 10 were intact, with no evidence for alternative splicing (Figure S2).

Discussion

This report describes an adult female patient of normal height who initially presented with a valgus deformity and later sustained multiple fractures, predominantly of the long bones. In childhood, her condition was debated, with dysosteosclerosis initially suspected due to bone sclerosis but later reclassified as Pyle disease because of a prominent metaphyseal widening and translucency. However, decades later, compound heterozygous mutations in the *TNFRSF11A* gene, which encodes the RANK receptor essential for osteoclast differentiation,[16] were identified, leading to a revised diagnosis of dysosteosclerosis.

Osteoclasts play a critical role in maintaining bone homeostasis, and impaired osteoclast function commonly results in sclerosing bone dysplasia.[3] The interaction between genetic and environmental factors influencing osteoclast activity is complex, resulting in a wide range of clinical presentations that can complicate diagnosis. Dysosteosclerosis can be differentiated from ARO by its milder osteosclerosis, lack of life-threatening progression, and distinct vertebral flattening and irregularities.[4] Biallelic mutations in *TNFRSF11A* can lead to both conditions, as well as familial expansile osteolysis (FEO; OMIM #174810).[17]

Our patient exhibits an unusually mild form of *TNFRSF11A*-associated skeletal dysplasia, characterized by normal height, slightly elevated BMD, and no generalized vertebral abnormalities, aside from mildly increased endplate opacity. She also presents with scoliosis, a feature not typically associated with *TNFRSF11A*-related conditions, and has experienced frequent fractures and distinct metaphyseal remodeling defects, both characteristic of dysosteosclerosis. The overlap of clinical features from dysosteosclerosis and Pyle disease, such as cortical bone thinning and metaphyseal widening, complicated the diagnosis. Given that her mother also has scoliosis, a polygenic contribution is suspected.

The history of our patient with multiple fractures from low-energy trauma suggests a greatly impaired bone quality. A markedly reduced serum concentration of the bone resorption marker CTx, alongside normal osteocalcin and slightly reduced P1NP serum concentrations, indicate an imbalance in bone remodeling likely due to impaired osteoclast function linked to the identified *TNFRSF11A* mutations. This is further supported by impaired *ex vivo* differentiation and function of osteoclast precursor cells obtained from the patient.

Autosomal dominant osteopetrosis (ADO; OMIM #166600), caused by *CLCN7* mutations, shares similarities

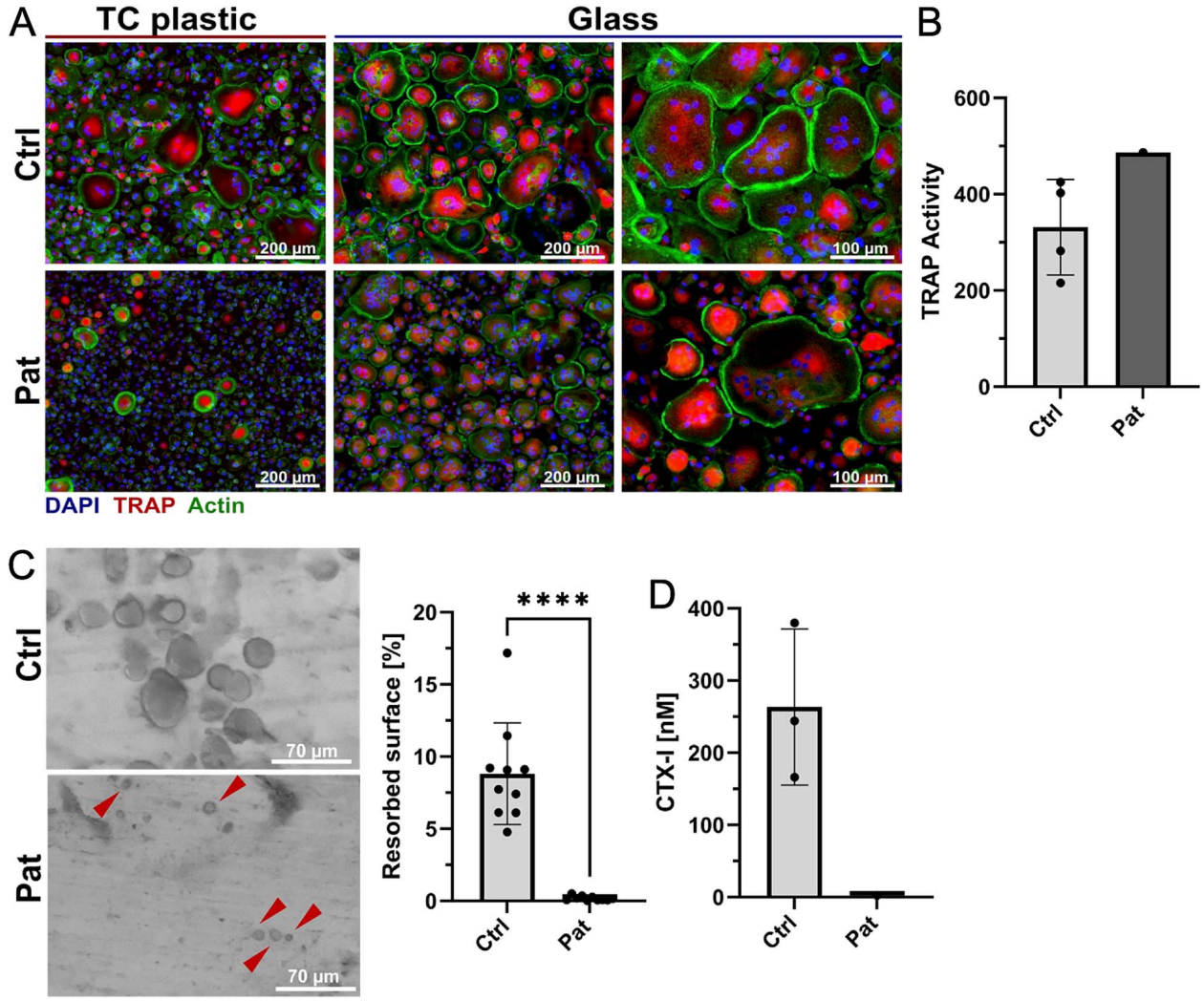

Figure 3. Delayed formation and impaired function of mutated osteoclasts. (A) Staining of control and patient osteoclast cultures demonstrated successful formation of osteoclasts on glass surfaces, but impaired formation on tissue-culture plastic. Nuclei are stained blue with DAPI, actin is stained green with phalloidin, and TRAP is shown in red through enzymatic staining. (B) Colorimetric analysis of TRAP activity in cell culture supernatants from bone resorption assays revealed no significant reduction in TRAP secretion ($n = 4$ controls, $n = 1$ patient-derived osteoclasts; single experiment) each point represents an individual measurements. (C) Representative images of resorption pits (indicated by red arrowheads) and quantification of eroded surfaces show minimal residual bone resorption compared to control cells (combined results from 3 independent experiments). (D) The release of CTx-I into cell culture supernatants from the bone resorption experiments, measured by ELISA, was significantly reduced in patient samples ($n = 3$ controls, $n = 1$ patient-derived osteoclasts, single experiment).

with dysosteosclerosis. However, in ADO, osteoclasts retain about 20% of their resorptive activity,[18,19] whereas osteoclasts in our patient appear more severely impaired. ADO typically presents with pronounced growth plate sclerosis and characteristic "sandwich" vertebrae, which were absent in our patient, who instead showed metaphyseal translucency and thin cortices. The increased growth plate opacity in ADO could be explained by the anabolic effects of partially active osteoclasts through coupling mechanisms.

Although the radiological phenotype in our patient suggests that osteoclasts can resorb mineralized growth plate cartilage, in vitro resorption was minimal. Notably, culturing osteoclasts on glass surfaces enhanced differentiation compared to plastic, consistent with previous findings that glass surfaces promote Src activation in osteoclasts.[20] We speculate that, beyond the essential differentiation factors M-CSF and RANKL, osteoclasts in vivo encounter additional stimuli that may enhance their formation, potentially explaining this discrepancy.

The most clinically comparable case of adult dysosteosclerosis associated with the homozygous *TNFRSF11A* variant c.784G>T in exon 9 was reported by Xue et al.[10] Despite introducing a premature termination codon (PTC), an alternative transcript with a milder in-frame deletion (p.E262_Q279del) resulted in a relatively mild phenotype, including short stature. In our patient, we identified the nonsense variant c.1093G>T (p.Glu365*) and the frameshift variant c.1266_1268delinsCC (p.Leu422Phefs*104) in *TNFRSF11A*. Among 29 known pathogenic *TNFRSF11A* variants, 15 are predicted to introduce a PTC, only 10 are missense mutations, 2 affect canonical splice sites, and one resides in the promoter.

All missense variants are linked to more severe ARO, except one identified in a dysosteosclerosis case. Since missense

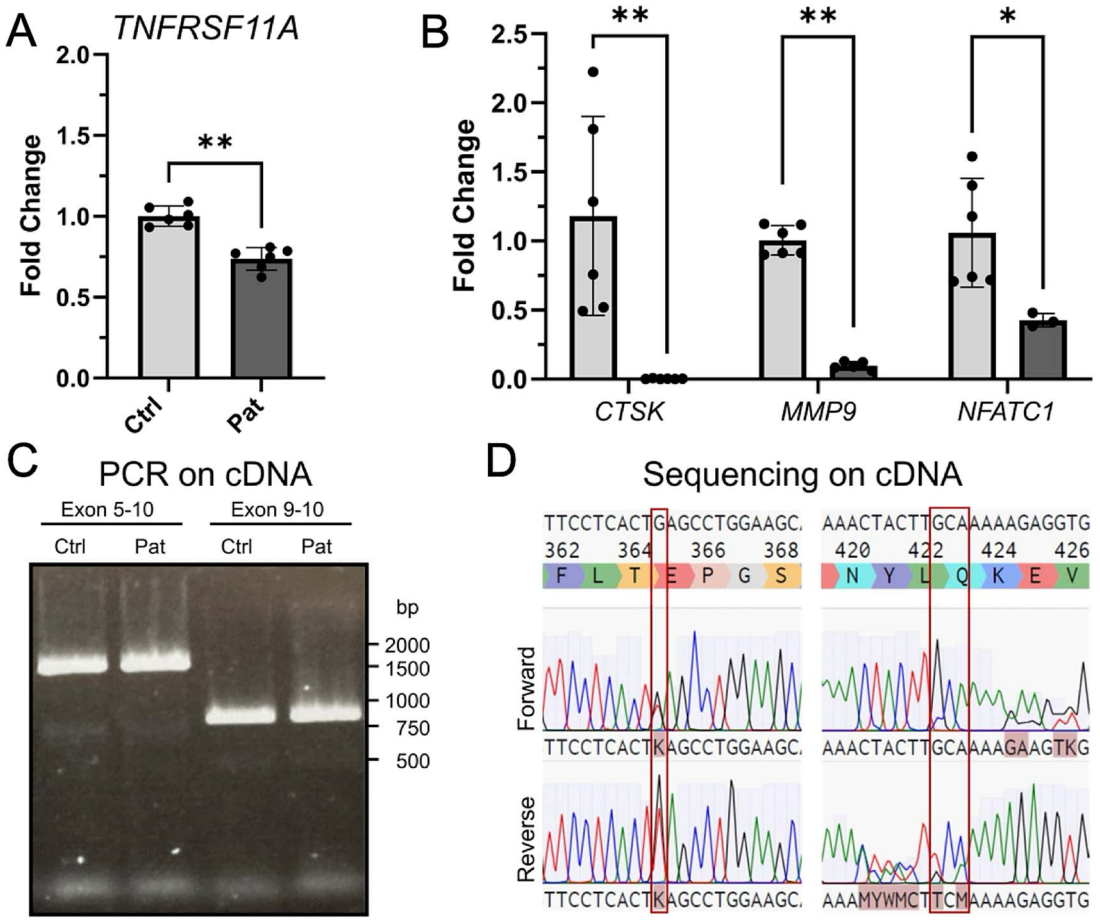

Figure 4. The primary transcript escapes NMD. (A) the fold change in *TNFRSF11A* expression was determined by qRT-PCR, showing only a slight reduction compared to the average expression in control samples. (B) the expression levels of osteoclast differentiation markers CTSK, MMP9, and NFATC1, also quantified by qRT-PCR, exhibited reduced expression associated with differentiation. Each point represents 3 technical replicates from 2 different control samples compared to technical replicates from patient samples. (C) Gel electrophoresis of amplified cDNAs from both control and patient samples revealed no significant secondary transcripts or splice abnormalities. (D) Sanger sequencing of the amplified cDNA confirmed the presence of both mutated mRNAs in a heterozygous state, suggesting that relevant nonsense-mediated decay (NMD) does not occur.

variants typically retain more protein function, PTC alleles generally result in more severe disease. However, PTCs in *TNFRSF11A* do not always induce complete loss-of-function (LOF).

PTC alleles are often targeted by NMD, but certain mechanisms allow them to escape this process.[21] In our patient, both variants (c.1093G>T and c.1266_1268delinsCC) are located in exon 9, a sufficiently large exon (784 bp) to evade NMD. Additionally, c.1266_1268delinsCC lies near the penultimate exon-intron junction, potentially enhancing its ability to escape NMD. Notably, 4 PTC-associated dysosteosclerosis variants are located in exons 9 or 10, and one is at the start of exon 1, also likely to evade NMD. The remaining variants affect splice sites or are missense mutations.

Our patient exhibits a paradoxical combination of osteosclerosis and osteopenia due to biallelic *TNFRSF11A* LOF variants that escape NMD. This complex condition necessitates a multidisciplinary treatment approach. Optimizing bone health through adequate vitamin D levels and calcium intake is essential, though the use of bone metabolism-altering drugs remains unsupported by evidence. Additionally, treating the patient's autoimmune thyroiditis is crucial, as thyroid hormones play a key role in bone metabolism.[22]

Future research may focus on elucidating the functional consequences of specific *TNFRSF11A* mutations on osteoclast differentiation and activity. A deeper understanding of the molecular mechanisms underlying dysosteosclerosis will enhance our understanding of bone metabolism and potentially identify targeted therapies to improve bone health.

In conclusion, this case illustrates the complexity of genetic defects affecting osteoclast function. The identification of compound heterozygous mutations in *TNFRSF11A* provides new insights into the pathogenesis of dysosteosclerosis.

Acknowledgments

We thank Jomêr Hamdosch for TRAP measurements and Claire Schlack for osteoclast quantifications.Uwe Kornak and Eric Hesse contributed equally.

Author contributions

Dario Gajewski: Experiments; data curation; analysis; visualization; manuscript review and editing. Anna Floriane Hennig: Experiments; data curation; analysis; visualization; manuscript review and editing. Regina Grün: Experiments; data curation; analysis; visualization; manuscript review and editing. Heide Siggelkow: Patient examination, manuscript review and editing. Svenja Vishnolia: Experiments;

data curation; analysis; visualization; manuscript review and editing. Leonard Bastian: Patient examination, manuscript review and editing. Hanna Taipaleenmäki: Data curation; visualization, manuscript review and editing. Ansgar Schulz: Patient examination, manuscript review and editing. Uwe Kornak: Conceptualization; genetic analysis; data curation; analysis; visualization; supervision; manuscript writing—review and editing. Eric Hesse: Conceptualization; patient examination; data curation; analysis; visualization; supervision; manuscript writing—review and editing.

Dario Gajewski (Data curation, Formal analysis, Investigation, Visualization, Writing—review & editing), Anna Henning (Data curation, Formal analysis, Investigation, Visualization, Writing—review & editing), Regina Grün (Data curation, Formal analysis, Investigation, Visualization, Writing—review & editing), Heide Siggelkow (Investigation, Writing—review & editing), Svenja Vishnolia (Data curation, Formal analysis, Investigation, Visualization, Writing—review & editing), Leonard Bastian (Investigation, Writing—review & editing), Hanna Taipaleenmäki (Data curation, Visualization, Writing—review & editing), Ansgar Schulz (Investigation, Writing—review & editing), Uwe Kornak (Conceptualization, Data curation, Formal analysis, Investigation, Project administration, Resources, Supervision, Validation, Visualization, Writing—original draft, Writing—review & editing), and Eric Hesse (Conceptualization, Data curation, Formal analysis, Investigation, Project administration, Resources, Supervision, Validation, Visualization, Writing—original draft, Writing—review & editing).

Supplementary material

Supplementary material is available at *JBMR Plus* online.

Funding

This research did not receive any grants or specific funding.

Conflicts of interest

All authors declare no conflict of interest and no competing financial interests.

Data availability

The data that support the findings of this study are available from the corresponding author upon reasonable request.

References

1. Veis DJ, O'Brien CA. Osteoclasts, master sculptors of bone. *Annu Rev Pathol*. 2024;18:257-281.
2. Sobacchi C, Schulz A, Coxon FP, Villa A, Helfrich MH. Osteopetrosis: genetics, treatment and new insights into osteoclast function. *Nat Rev Endocrinol*. 2013;9(9):522-536. https://doi.org/10.1038/nrendo.2013.137
3. Bergen DJM, Maurizi A, Formosa MM, et al. High bone mass disorders: new insights from connecting the clinic and the bench. *J Bone Miner Res*. 2023;38(2):229-247. https://doi.org/10.1002/jbmr.4715
4. Turan S. Osteopetrosis: gene-based nosology and significance dysosteosclerosis. *Bone*. 2023;167:116615. https://doi.org/10.1016/j.bone.2022.116615
5. Whyte MP, Wenkert D, McAlister WH, et al. Dysosteosclerosis presents as an "osteoclast-poor" form of osteopetrosis: comprehensive investigation of a 3-year-old girl and literature review. *J Bone Miner Res*. 2010;25(11):2527-2539. https://doi.org/10.1002/jbmr.131
6. Simsek Kiper PO, Saito H, Gori F, et al. Cortical-bone fragility—insights from sFRP4 deficiency in Pyle's disease. *N Engl J Med*. 2016;374(26):2553-2562.
7. Pangrazio A, Cassani B, Guerrini MM, et al. RANK-dependent autosomal recessive osteopetrosis: characterization of five new cases with novel mutations. *J Bone Miner Res*. 2012;27(2):342-351. https://doi.org/10.1002/jbmr.559
8. Guerrini MM, Sobacchi C, Cassani B, et al. Human osteoclast-poor osteopetrosis with hypogammaglobulinemia due to TNFRSF11A (RANK) mutations. *Am J Hum Genet*. 2008;83(1):64-76. https://doi.org/10.1016/j.ajhg.2008.06.015
9. Guo L, Elcioglu NH, Karalar OK, et al. Dysosteosclerosis is also caused by TNFRSF11A mutation. *J Hum Genet*. 2018;63(6):769-774. https://doi.org/10.1038/s10038-018-0447-6
10. Xue JY, Wang Z, Shinagawa S, et al. TNFRSF11A-associated dysosteosclerosis: a report of the second case and characterization of the phenotypic spectrum. *J Bone Miner Res*. 2019;34(10):1873-1879. https://doi.org/10.1002/jbmr.3805
11. Kırkgöz T, Özkan B, Hazan F, et al. A null mutation of TNFRSF11A causes dysosteosclerosis, not osteopetrosis. *Front Genet*. 2022;13:928814. https://doi.org/10.3389/fgene.2022.938814
12. Oheim R, Tsourdi E, Seefried L, et al. Genetic diagnostics in routine osteological assessment of adult low bone mass disorders. *J Clin Endocrinol Metab*. 2022;107(7):E3048-E3057. https://doi.org/10.1210/clinem/dgac147
13. Hombach D, Schuelke M, Knierim E, et al. MutationDistiller: user-driven identification of pathogenic DNA variants. *Nucleic Acids Res*. 2019;47(W1):W114-W120. https://doi.org/10.1093/nar/gkz330
14. Schwarz JM, Rödelsperger C, Schuelke M, Seelow D. MutationTaster evaluates disease-causing potential of sequence alterations. *Nat Methods*. 2010;7(8):575-576. https://doi.org/10.1038/nmeth0810-575
15. Richards S, Aziz N, Bale S, et al. Standards and guidelines for the interpretation of sequence variants: a joint consensus recommendation of the American College of Medical Genetics and Genomics and the Association for Molecular Pathology. *Genet Med*. 2015;17(5):405-424. https://doi.org/10.1038/gim.2015.30
16. Dougall WC, Glaccum M, Charrier K, et al. RANK is essential for osteoclast and lymph node development. *Genes Dev*. 1999;13(18):2412-2424. https://doi.org/10.1101/gad.13.18.2412
17. Hughes AE, Ralston SH, Marken J, et al. Mutations in TNFRSF11A, affecting the signal peptide of RANK, cause familial expansile osteolysis. *Nat Genet*. 2000;24(1):45-48. https://doi.org/10.1038/71667
18. Supanchart C, Wartosch L, Schlack C, et al. ClC-7 expression levels critically regulate bone turnover, but not gastric acid secretion. *Bone*. 2014;58:92-102. https://doi.org/10.1016/j.bone.2013.09.022
19. Polgreen LE, Imel EA, Econs MJ. Autosomal dominant osteopetrosis. *Bone*. 2023;170:116723. https://doi.org/10.1016/j.bone.2023.116723
20. Hu B, Chen Y, Li Y, et al. Substrate-mediated regulation of Src expression drives osteoclastogenesis divergence. *Genes (Basel)*. 2024;15(9):1-16. https://doi.org/10.3390/genes15091217
21. Lindeboom RGH, Vermeulen M, Lehner B, Supek F. The impact of nonsense-mediated mRNA decay on genetic disease, gene editing and cancer immunotherapy. *Nat Genet*. 2019;51(11):1645-1651. https://doi.org/10.1038/s41588-019-0517-5
22. Delitala AP, Scuteri A, Doria C. Thyroid hormone diseases and osteoporosis. *J Clin Med*. 2020;9(4):1-18. https://doi.org/10.3390/jcm9041034

JBMR Plus, 2025, 9, ziae179
https://doi.org/10.1093/jbmrpl/ziae179
Case Report